Spinal neural tube formation and tail development in human embryos

Chloe Santos *, Abigail R. Marshall *, Ailish Murray [1]*, Kate Metcalfe, Priyanka Narayan, Sandra C. P. de Castro, Eirini Maniou, Nicholas D. E. Greene, Gabriel L. Galea and Andrew J. Copp [2]

Developmental Biology & Cancer, UCL Great Ormond Street Institute of Child Health, 30 Guilford Street, London WC1N 1EH, UK

* These authors contributed equally to the study

[1] Current address: Moorfields Eye Charity, 162 City Road, London, EC1V 2PD

[2] Author for correspondence: tel: +44 207 905 2355; e-mail: a.copp@ucl.ac.uk

ABSTRACT

Formation of the nervous system in the spinal region of higher vertebrates involves primary and secondary neurulation, in which the neural tube forms by closure and canalisation respectively. These processes are incompletely understood in humans, in part due to the challenge of accessing neurulation-stage embryos (3-7 weeks post-conception). Here we present findings on completion of primary neurulation and formation of the 'secondary body' (including secondary neurulation) in 108 human embryos that span Carnegie Stages (CS) 10 to 18. Several outstanding questions on low spinal development in humans are addressed: we show that primary neurulation is completed at the human posterior neuropore with a pattern of neural plate bending similar to that in the mouse. There is no evidence of a 'transition zone' to secondary neurulation, which proceeds from CS13 with formation of a single lumen as in mouse, not coalescence of multiple lumens as has been claimed based on chick neurulation. Secondary neural tube 'splitting' is seen in the more proximal tail regions of 60% of human embryos. A somite is formed every 7 h in human, compared with 2 h in mice and a 5 h 'segmentation clock' in human organoids. Termination of axial elongation occurs after downregulation of *WNT3A* and *FGF8* in the CS15 embryonic tailbud, with a 'burst' of apoptosis that may remove the neuro-mesodermal progenitors. We conclude that low spinal neurulation and secondary body formation follow a similar pattern in humans as in mammalian model systems such as mouse and rat. Investigators are now attempting to recapitulate events of neurulation in organoids derived from human stem cells, and our findings provide 'normative data' for interpretation of such in vitro results.

INTRODUCTION

Development of the lumbosacral spinal cord is a critical period of embryogenesis. Not only does motor control and sensation in the legs and lower body depend on this event, but proper functioning of bladder, rectum and genital organs are all critically dependent on nerves arising from the low spinal cord. A major group of congenital malformations termed neural tube defects (NTDs) result when low spinal neurulation fails to be completed or is otherwise abnormal, and these can be open or closed (skin-covered) lesions.

Open spina bifida (also called myelomeningocele) results from defective closure of the primary neural tube, most often at lumbar and upper sacral levels. Subsequent neuroepithelial loss due to prolonged exposure to amniotic fluid (Stiefel et al., 2007) leads to a defect that is disabling in most individuals (Copp et al., 2015). Closed ‘dysraphic’ conditions arise at lower sacral and coccygeal levels of the body axis and result from disturbance of secondary neurulation, in which the neural tube forms without formation of neural folds. Dysraphic conditions involve an abnormal anatomical relationship between the secondary neural tube and surrounding tissues, often with ectopic adipose tissue, as in spinal lipoma and lipomyelomeningocele (Jones et al., 2019). Closed dysraphism may be asymptomatic, but significant disability can occur through tethering of the low spinal cord to non-neural tissues (Agarwalla et al., 2007).

In normal primary and secondary neurulation, the neural tube forms by closure and canalisation respectively (summarised in Figure 1 of Nikolopoulou, 2017), with extensive studies of both processes in experimental animals, especially chick, mouse and rat. Despite the relative inaccessibility of neurulation-stage human embryos (3-7 weeks post-conception), a number of studies have described the anatomical, histological and ultrastructural features of secondary neurulation (Supplementary Table 1). Although limited molecular research has been performed, e.g. to determine the mode of cell death in human tail regression (Vilovic et al., 2006), a few studies have begun to address specific gene expression during human secondary body

development (Olivera-Martinez et al., 2012; Yang et al., 2014). Increasingly, transcriptomic approaches are being used with organogenesis-stage human embryos (Fang et al., 2010; Yi et al., 2010; Krupp et al., 2012; Xu et al., 2023).

Caudal development comprises not only formation of the secondary neural tube, but also other tissue types within the 'secondary body' region. This part of the body axis – beyond the cloacal plate which marks the future anus – includes the secondary notochord, tail somites, caudal vessels, tailgut and surrounding surface ectoderm (future epidermis). These structures show marked tissue-to-tissue variation in development. For example, tail regression in human embryos involves loss of all tail components, whereas the rodent tail maintains the somites and notochord, but loses the secondary neural tube and tailgut. The regulation of this balance between maintenance and loss of tail structures is not understood.

A related area of interest is the molecular control of axial elongation. A population of self-renewing stem cells, termed neuro-mesodermal progenitors (NMPs), resides in the caudal-most embryonic region (the tailbud), with NMPs giving rise to neural and mesodermal derivatives, including the secondary neural tube and somites (Henrique et al., 2015). NMP maintenance is required for axial elongation, mediated via an interplay between WNT3A and FGF8 expression, which promotes NMP survival in the tailbud. Conversely, endogenous retinoic acid promotes differentiation and regulates body length (Wilson et al., 2009).

In the present study, we examined caudal development in 108 human embryos, at Carnegie Stages (CS)10-18 (3.5-6.5 weeks post-conception). The aim was to gain new information on several unanswered or controversial questions in human neurulation, including: (i) how the embryo transitions from primary to secondary neurulation; (ii) the mode of formation of the secondary neural tube; (iii) the rate of somite formation during low spinal development; (iv) the possible roles of WNT3A and FGF8 in regulating axial elongation; (v) whether a 'burst' of apoptosis coincides with termination of axial elongation. A further aim was to gather and present findings on human

spinal neurulation that can serve as ‘normative data’ to aid interpretation of research involving multicellular ‘organoid’ structures, that are being increasingly used to model various aspects of human axial development (Denham et al., 2015; Fedorova et al., 2019; Moris et al., 2020; Rifes et al., 2020; Karzbrun et al., 2021; Libby et al., 2021; Amadei et al., 2022).

RESULTS

The study involved 108 human embryos (Table 1), obtained from the MRC/Wellcome Human Developmental Biology Resource (www.hdbr.org), with UK ethics committee approval. Embryos were donated by women undergoing termination of pregnancy for 'social' reasons, in most cases by mifepristone/misoprostol-induced (medical) delivery, with a few intact embryos obtained by ultrasound-guided vacuum aspiration (surgical). All embryos in the study were chromosomally and morphologically normal, and were assigned to Carnegie Stages (CS), as described (O'Rahilly and Muller 1987; Bullen and Wilson 1997). Comparisons to mouse were with random-bred CD1 embryos, staged by embryonic (E) day, where E0.5 is the day following overnight mating.

Morphology of human posterior neuropore (PNP) closure

Relatively few human embryos with an open PNP have been reported in the literature (Müller and O'Rahilly 1987; O'Rahilly and Müller 2002), probably owing to the early stage at which primary neurulation is completed (end of week 4, post-conception). In two intact CS12 embryos (Figure 1A,B; crown-rump length: 3 mm; 22-23 somites), we identified an open PNP by microscopic inspection at collection (Figure 1C,D). Transverse histological sections confirmed an open neural tube in the caudal region, with minimal tissue damage evident, indicating that primary neurulation was not yet complete. The neural plate is relatively flat in the most caudally located sections, although incipient dorsolateral hinge points (DLHPs) are visible (Figure 1E,F). The notochord underlies the neural plate midline, and the caudal end of the hindgut is visible beneath the notochord in one embryo (Figure 1E), but not the other (Figure 1F). In more rostral sections, close to the 'zippering' point of PNP closure, elevated neural folds flank a marked ventral midline bend in the neural plate, the median hinge point (MHP), which precisely overlies the notochord (Figure 1G,H). DLHPs are also clearly present, unilaterally in one embryo (Figure 1G) and bilaterally in the other (Figure 1H). As in the mouse (McShane et al., 2015), the DLHPs are situated where the neural plate changes from basal contact with surface ectoderm to basal contact with paraxial mesoderm. We conclude that MHP and DLHPs characterise PNP closure in human embryos at

CS12, marking a direct equivalence to Mode 2 spinal neurulation in the mouse embryo (Shum and Copp 1996).

Timing of human PNP closure

PNP length data were obtained from photographic images of CS10-CS13 embryos (n = 40). To allow for differences in overall embryonic size, PNP measurements were normalised to the length of a recently formed somite in the same embryo (Figure 1C). The plot of PNP length/somite length against somite number shows a steady decline in the length of open neural folds in the caudal region, until 6/12 embryos at CS13 have completely closed, while most of the others show a very small PNP (Figure 1I). There were no obvious differences in closure rate or timing between female (n = 24) and male (n = 16) embryos. Hence, closure of the PNP is completed in human embryos around the 30-somite stage, as also reported for outbred mouse strains (Copp et al., 1982).

Development and regression of the human embryonic tail

Overall caudal development was studied in 37 human embryos (CS13-CS18), which covered the period 28-45 days post-conception (Table 2; Figure 2A,B,I). Crown-rump length increased 2.5-fold during this period, from a mean value of 6.4 mm at CS13 to 15.4 mm at CS18 (Table 2; Figure 2J). Observations on the intact embryos showed that the PNP is closed in most embryos by CS13, and a developing tailbud is present which exhibits mild ventral curvature and a thick rounded tip (Figure 2C). Somites are visible proximal to the tailbud (arrowheads in Figure 2C), with an intervening region of presomitic mesoderm at CS13 (yellow bracket in Figure 2C). By CS16, however, the somites extend almost to the tail tip (yellow arrow in Figure 2F). As development progresses, striking changes occur in the tail which continues to lengthen (Table 2) but simultaneously narrows, particularly at the tip, to yield a sharply pointed structure by CS16 (Figure 2D-F). At the same time, the tail straightens and even becomes dorsally bent (Figure 2F). Subsequent to CS16, the tail shortens (Figure 2G; Table 2), and its distal portion becomes increasingly translucent in appearance. By CS18, only a short, curved stump remains (Figure 2H), and the tail is lost

completely thereafter. Additional embryonic tails in the CS13-CS18 range are shown in Supplementary Figure 1.

Somite formation

Between CS10 and CS13, during PNP closure, somite number increases approximately linearly with days of gestation (Figure 1K): mean (± SD) somite numbers were: 8.0 ± 1.4 at CS10, 18.4 ± 2.6 at CS11, 23.5 ± 3.4 at CS12 and 30.0 ± 2.8 at CS13. The linear regression equation of this relationship (Figure 1K) gives an increase of 20.3 somites over a 6-day period, equating to the formation of 3.4 somites per gestational day, or a new somite every 7.1 h (95% confidence intervals: 4.8, 10.4). This compares with formation of a new somite every 2 h in rat and mouse embryos (Brown and Fabro 1981; Tam 1981), and a 5 h periodicity observed for the human 'in vitro segmentation clock' in stem cell-derived presomitic mesoderm-like cells (Diaz-Cuadros et al., 2020; Matsuda et al., 2020). Following PNP closure at CS13, the largest somite number was at CS16 (36.6 ± 1.2; Table 2), although there was no statistically significant increase between CS13 and CS16 (Figure 2K). By CS17 and 18, we could identify only 31-34 somites, a significant reduction in number (Figure 2K). Hence, somite formation in humans occurs at a rate that is 3.5-times slower than in rodent embryos, and ceases after CS16. Subsequent somite number reduction suggests that shortening of the tail during regression involves loss of somites (Table 2).

Mode of cell death during tail regression

In an initial study, transverse histological sections through human and mouse embryonic tails were processed for immuno-peroxidase staining using anti-activated caspase 3. Positive cells were readily identified in the tails of both species (Figure 3A-N), arguing for a role of caspase-dependent apoptosis during tail regression in human and mouse. Principal sites of apoptotic cell death include the regressing tailgut (Figure 3D,F) and, most abundantly, the ventral mesoderm overlying the epithelial ventral ectodermal ridge (Figure 3C,E). We also detected TUNEL-positive cells in both mouse and human tail sections (data not shown), further confirming the presence of apoptotic cells during tail development/regression.

A burst of apoptosis at cessation of tail elongation

We observed enhanced apoptosis in the mouse tailbud at E13.5 (Figure 3J), compared with E13.0 and E14.0 when relatively few dying cells were present (Figure 3I,K). Similarly, in sections through the caudal-most region of human embryos, apoptosis was not observed at CS13 (Figure 3L), became intense at CS15 (Figure 3M), and diminished in intensity by CS18 (Figure 3N). Hence, in both mouse and human tails, there appears to be a 'burst' of apoptosis at the stage when tail growth ceases, and just before regression of internal structures gets underway.

Evidence for regression of the tailgut from rostral to caudal

While the human embryonic tail appears to regress from caudal to rostral (Figure 2), the proximal (rostral) part of the tailgut is reported to degenerate before the more distal (caudal) part in both rat (Butcher 1929; Qi et al., 2000) and mouse (Nievelstein et al., 1993a; Nievelstein et al., 1993b). To examine this question in human embryos, we performed immunofluorescence for anti-activated caspase 3, which confirmed the presence of apoptosis in both tailgut and ventral mesoderm (Figure 4A',B'). Using DAPI-stained sections along the secondary body axis (Figure 4A,B), we determined the cross-sectional area of neural tube, notochord and tailgut in two CS14 and one CS15 embryos. Total tail area served as a measure of axial position. The neural tube showed a progressive increase in area towards the proximal (rostral) end of the tail, while the notochord showed no change in area along the body axis (Figure 4C). Strikingly, the tailgut showed the reverse trend, with a marked caudal-to-rostral reduction in cross-sectional area (Figure 4A,B,D). Tailgut nuclear number also diminished from caudal to rostral (Figure 4E). Hence, although the rostral tailgut has not disappeared by CS15, it appears to be diminishing in size proximally, at the same time as it is being formed, as a prominent tail structure, caudally. We conclude that rostral-to-caudal loss of the tailgut may be a general phenomenon among mammalian embryos.

Expression of *FGF8* and *WNT3A* during human tailbud elongation

To begin an assessment of the mechanisms that may regulate elongation of the human embryonic tail, and its cessation, we performed whole mount in situ hybridisation for *FGF8* and *WNT3A* (n = 2 embryos minimum for each gene at each stage). These genes are developmentally regulated during axial elongation in chick and mouse embryos, with strong expression in the tailbud during elongation, and down-regulation before axial growth ceases. Direct inactivation or indirect down-regulation of the genes leads to premature axial truncation (Wilson et al., 2009).

In accordance with these findings, we observed strong expression of *FGF8* in the tailbud at CS12 and CS13, as revealed in whole embryos (Figure 5A,B) and longitudinal sections through hybridised caudal regions (Figure 5E,F). At CS14, *FGF8* expression reduced dramatically so that only a small 'dot' of expression was detected in the tailbud (Figure 5C,G), and by CS15 expression of *FGF8* was no longer detectable in the tail (Figure 5D,H). Expression of *WNT3A* followed a similar pattern with strong expression in the tailbud at CS12 (Figure 5I,M), reduced expression intensity at CS13 (Figure 5J,N), a remaining 'dot' of tailbud expression at CS14 (Figure 5K,O), and no detectable *WNT3A* expression in the tail at CS15 (Figure 5L,P). We conclude that expression of *FGF8* and *WNT3A* mirrors the relationship seen in mouse and chick, with strong tailbud expression during active axial extension, and dramatic down-regulation of both genes before the onset of axial growth cessation. It is striking that down-regulation appears complete by CS15, even though the embryonic tail does not reach its maximum length until some days later, at CS16 (Table 2). Down-regulation of *Fgf8* and *Wnt3a*, well in advance of cessation of axial elongation, has also been observed in mouse embryos (Cambray and Wilson 2007).

Mode of secondary neural tube formation in human embryos

In our initial study of tail morphology, 9 out of 15 human embryonic tails showed multiple lumens in some transverse sections (Figure 3G,H), whereas the other 6 exhibited only a single neural tube lumen. In a second group of serially sectioned tails (Figures 4,6), 6 out of 10 tails had regions of duplicated neural tube. Hence, we find a 60% (15/25) frequency of neural tube duplication,

confirming previous findings of multiple neural tube lumens in many human embryonic tails (Bolli 1966; Lemire 1969; Saitsu et al., 2004). We most often identified two neural tube profiles in a single transverse section, but in some cases more were observed (e.g. at CS15; Figure 3G).

These initial findings of neural tube duplication prompted a more detailed examination of the suggestion that multiple neural tube lumens represent a mode of human secondary neurulation similar to that seen in the avian embryo (Lemire 1969; Saitsu et al., 2004; Pang 2020). In chick, multiple lumens form distally in the tail bud, and coalesce more rostrally to form the secondary neural tube (Criley 1969; Schoenwolf and De Longo 1980; Yang et al., 2003; Gonzalez-Gobartt et al., 2021). An alternative view would be that multiple lumens arise only later in human secondary body formation (Catala 2021), perhaps representing splitting of the already formed secondary neural tube (Figure 6A).

To help resolve this issue, we asked two questions: (i) what is the status of the secondary neural tube where it is first formed, close to the tailbud tip? (ii) at what level of the tail axis is neural tube duplication most often seen? In our initial series of human tails, a single lumen was invariably noted in the distal-most portion of the neural tube, just rostral to the tailbud tip (CS13-18; Figure 3L-N). This was confirmed in the second series of ten serially sectioned tails (CS14-15; Figure 6B,C,D), thus demonstrating that secondary neurulation in human produces a neural tube with a single lumen. When multiple secondary neural tube lumens were visible in the embryonic tail, this was invariably located at more rostral levels of the tail (Figure 3G,H; Figure 4C; Figure 6B’,C’’,D’’), with variation in location between embryos. We conclude that multiple secondary neural tube lumens in human embryonic tails likely represent splitting, which tends to occur rostrally and does not represent a secondary neurulation mechanism involving coalescence of multiple lumens, as in chick. Humans therefore resemble other mammals, including rat and mouse, in initially forming a single secondary neural tube lumen in the tail-bud.

DISCUSSION

The development and later disappearance of the human tail has been of interest to embryologists for more than a century (Catala 2021). To better appreciate the knowledge base for human embryonic caudal development, we conducted a systematic literature review using several search terms (see Materials and Methods). This generated a long-list of publications that was filtered to include only those with primary data relating to caudal development in human embryos. The final list comprises 28 papers (Supplementary Table 1) that span over 100 years of research, from the early 1900s (Kunitomo 1918; Streeter 1919) to recent times (Xu et al., 2023). This work was based on at least 925 human embryos obtained from varying sources (Supplementary Table 1) including induced termination of pregnancy for 'social' reasons (where most embryos are expected to be normal), as well as spontaneous abortion (miscarriage) and ectopic pregnancy, where embryonic abnormalities are likely to be frequent. Hence, interpretation of embryo morphology in these studies needs to take into account the mode of procurement of the human specimens.

Several aspects of caudal development are addressed by the studies in Supplementary Table 1. These include: completion of primary neurulation with PNP closure, the transition into secondary neurulation, the mode of formation and regression of the secondary neural tube, the observation of multiple neural tube lumens, the formation and regression of somites, notochord and gut in the tail region, the role of programmed cell death in tail regression, and initial studies of gene expression in human embryos. Taken together with the findings of the present study, this accumulated literature provides a strong morphological evidence base for 'in vivo' human caudal development, against which in vitro studies can be judged in the emerging field of stem cell-derived organoid differentiation. The latter is producing multicellular structures that may ultimately provide experimentally tractable models for some aspects of human axial development (Denham et al., 2015; Fedorova et al., 2019; Moris et al., 2020; Rifes et al., 2020; Karzbrun et al., 2021; Libby et al., 2021; Amadei et al., 2022).

Concept of a human ‘tail’

The human tail develops and then regresses during weeks 4-7 post-conception and is composed of a secondary neural tube, notochord, somites and tailgut, with undifferentiated mesenchyme at its tip (the tailbud or ‘caudal eminence’), all within a surface ectoderm covering. Since it never becomes vertebrated, in contrast to the tails of most other mammals, some authors consider the human caudal appendage does not qualify as a ‘tail’ (Müller and O'Rahilly 2004). On the other hand, the presence of caudal somites with vertebra-forming potential are considered by other authors to endow the human caudal appendage with all the hallmarks of a mammalian tail (Kunitomo 1918). In keeping with common usage, we have referred to the transient human caudal appendage as a tail in this paper. Moreover, we note that the recent claim of ‘tail-loss’ during human evolution, due to a genetic change in the *TBXT* gene (Xia et al., 2024), ignores the fact that tail development persists in humans, albeit during a specific stage of embryonic development.

Transition from primary to secondary neurulation

Primary neurulation ends with completion of PNP closure, which we detect at the 30-somite stage in humans, similar to mice (Van Straaten et al., 1992). In mouse embryos, three sequential Modes of spinal neurulation occur (Shum and Copp 1996): in Mode 1, the upper spinal neural plate bends only at the midline (the median hinge point; MHP); in Mode 2, at intermediate spinal levels, bending is at both MHP and paired dorsolateral hinge points (DLHPs); in Mode 3, immediately before final PNP closure, the MHP is lost and bending occurs only at DLHPs. We found that PNP closure is complete in most CS13 human embryos, and that two CS12 embryos exhibit both MHP and DLHPs in their PNPs. This raises the possibility that ‘Mode 2’ neural plate bending is typical of the late stages of human spinal neurulation, and that ‘Mode 3’ is mouse-specific and not seen in humans. Alternatively, our CS12 embryos may have been developmentally too early to show Mode 3 closure. Analysis of further human embryos with open PNPs should resolve this question.

Our sectioning analysis along the body axis of CS14-CS15 human embryos revealed continuity of the neural tube from proximal (primary neurulation) to distal (secondary neurulation) levels. Indeed,

it was not possible to locate with any certainty where the transition from primary to secondary neural tube had occurred. This closely resembles the mouse (Shum and Copp 1996), but contrasts with the chick where a ‘transition zone’ occurs between primary and secondary neurulation. The chick primary (dorsal) and secondary (ventral) neural tubes overlap for a short length of the spinal axis (Dryden 1980) and cells ingressing at the node-streak border participate in a distinct ‘junctional neurulation’ process with essential function of the *Prickle-1* gene (Dady et al., 2014). Human ‘junctional neurulation’ has also been invoked as an explanation for an unusual form of spinal dysraphism where primary and secondary neural tubes are physically and functionally separated from each other, with no intervening neural tissue (Eibach et al., 2016). However, the lack of any evidence for ‘junctional neurulation’ in the present study of human embryos casts doubt on the proposed developmental origin of this rare dysraphic defect.

Mode of development of the human secondary neural tube

Secondary neurulation in mouse and rat involves formation of a single ‘rosette’ structure caudally, in which cells aggregate (‘condense’) from the dorsal tailbud mesenchyme, with subsequent (more rostral) organisation of the cells around a single lumen. This process is driven by apical junction formation, not by cell death (Butcher 1929; Schoenwolf 1984; Kostovic-Knezevic et al., 1991; Nievelstein et al., 1993b). In chick, by contrast, a caudal-to-rostral sequence of events occurs in which several independent lumens arise in the dorsal tailbud mesenchyme and, at more rostral levels, these coalesce to form the single lumen of the secondary neural tube (Criley 1969; Schoenwolf and De Longo 1980; Yang et al., 2003). Coalescence is a cell intercalation process driven by TGFβ/SMAD3 signalling (Gonzalez-Gobartt et al., 2021).

The mode of formation of the human secondary neural tube is controversial. Multiple neural tube lumens have often been observed in the developing or regressing tail (Bolli 1966; Lemire 1969; Hughes and Freeman 1974; Fallon and Simandl 1978; Saitsu et al., 2004; Pytel et al., 2007; Yang et al., 2014), whereas other studies identify only a single lumen (Müller and O'Rahilly 1987; Nievelstein et al., 1993b). Here, we found multiple secondary neural tube lumens in 60% of human

embryos. An important question is whether such multiple lumens are part of the normal secondary neurulation process in humans – thus making the human more similar to chick than mouse, as has been claimed (Pang 2020). Alternatively, multiple lumens could arise through later ‘splitting’ of the previously formed neural tube. In mice, neural tube duplication is part of several mutant phenotypes and, when present, is a sign of pathology (Cogliatti 1986).

A limitation of previous studies is the paucity of information on the morphology of the secondary neural tube at specific rostro-caudal axial levels. To shed light on this question, we examined human embryonic tails with the aim of determining the axial sequence of secondary neurulation events. Our findings show that multiple lumens, if present, feature at relatively rostral (mature) levels of the secondary neural tube and are absent from the most caudal (immature) levels, close to the tailbud. This applies to embryos throughout the secondary neurulation process (CS13-17), and argues strongly against coalescence of chick-like multiple lumens as a feature of normal human secondary neurulation. A recent review has drawn the same conclusion (Catala 2021). Hence, ‘splitting’ of the human secondary neural tube appears a common but not obligatory phenomenon, perhaps reflecting changes related to tail regression.

Tailgut: origin and mode of regression

The tailgut is an extension of the hindgut, beginning caudal to the level of the cloacal plate (future anus), which is located ventral to somite 29 in the mouse (Nievelstein et al., 1993a). The tailgut forms and then regresses in both tailed (mouse, rat) and non-tailed (chick, human) animals. Interestingly, human tailgut loss has been described as involving rostral-to-caudal degeneration rather than a more intuitive caudal-to-rostral loss (Kunitomo 1918; Fallon and Simandl 1978). Consistent with this, the tailgut lumen persists longest at the tail tip in rat (Butcher 1929; Qi et al., 2000) and mouse (Nievelstein et al., 1993a). Our finding of a rostral-to-caudal diminution in tailgut size and cell number is consistent with tailgut loss at rostral before caudal levels also in human embryos.

In contrast to the consensus on tailgut regression, there is disagreement over the developmental origin of the tailgut. Anatomical and histological studies in rat, mouse and human often conclude that the tailgut originates by mesenchyme-to-epithelium transition of tailbud cells, in a manner similar to the origin of the secondary neural tube (Svajger et al., 1985; Gajovic et al., 1989; 1993; Nievelstein et al., 1993b). However, others consider the tailgut to arise by caudally directed extension of the hindgut (Jolly and Ferester-Tadie 1936). Grafting of the E10.5 mouse tailbud beneath the kidney capsule produced no evidence of gut epithelial differentiation, in contrast to primitive streak/tailbud fragments at E8.5 and E9.5 which regularly produced this derivative. This finding is consistent with loss of gut-forming potential in the later stage tailbud (Tam 1984).

The question of tailgut origin can also be considered in light of the identification of NMPs: the stem cell population for tissues of the caudal embryonic region (Wilson et al., 2009; Wymeersch et al., 2021). A retrospective clonal analysis found gut endoderm only as part of rostrally-derived clones, unlike neural tube and paraxial mesoderm that were represented in clones extending into the tailbud at E10.5 (Tzouanacou et al., 2009). This led to the idea that NMPs are bipotential, forming neural and paraxial mesodermal derivatives, whereas the endodermal lineage is set aside separately, early in gastrulation. These findings are consistent with results of DiI-based lineage tracing and tissue grafting experiments (Cambray and Wilson 2002; 2007) which show that the NMP population at the chordoneural hinge region (CNH) of the tailbud is fated to form neural and mesodermal derivatives, but not tailgut. Further support for this concept comes from the finding of a proliferative zone at the hindgut tip, which is required to generate the colon by caudally directed gut extension (Garriock et al., 2020). It will be interesting to determine whether a similar mechanism underlies tailgut development.

Mechanism of cessation of tail elongation

Termination of axial elongation is highly species-specific, occurring in embryos with fewer than 40 somites in human (Table 2), at ~ 52-somite stage in chick, and in embryos with 65 somites in rat and mouse (Olivera-Martinez et al., 2012). One question is whether the underlying molecular and

cellular mechanisms are shared, despite these variations in timing, or are fundamentally different between species. Our findings with human embryos support a shared mechanism, as we find that expression of *FGF8* and *WNT3A* are developmentally regulated in close relationship to the time-course of axial elongation, similar to that in rodent embryos. Moreover, cessation of tail growth in the mouse has been linked to a burst of apoptosis in the tailbud around E13.5 (Wilson et al., 2009), and we detected an analogous burst of apoptosis in the CS15 human tailbud. Hence, a similar mechanism may underlie growth termination of the much shorter human embryonic tail.

Type and timing of cell death during tail regression

While programmed cell death is recognised to participate in tail regression, the precise mode of cell death has been debated. In immunohistochemistry studies, it was concluded that apoptosis occurs only in the human cranial embryonic region, and non-apoptotic ('necrotic-like') death of tail structures was identified in the regressing human tail (Sapunar et al., 2001; Vilovic et al., 2006). In contrast, cell death during chick tail regression was shown to involve caspase-dependent apoptosis (Miller and Briglin 1996). Using anti-caspase 3 and TUNEL methods, we identified apoptosis in the human tail, with patterns of cell death occurring in a closely similar way between human and mouse embryos. We conclude that caspase-dependent apoptosis is the predominant mode of cell loss during tissue regression in the tails of both mouse and human.

Conclusions

The findings of this study show a close parallel between human and rodent embryos in several features of low spinal development: completion of primary neurulation, transition to secondary neurulation, cellular mechanism of secondary neural tube formation and molecular basis of cessation of tail elongation. In contrast, some aspects of chick low spinal development – often cited as an accurate model for human – are not represented in the human embryos, indicating the need for caution in extrapolating findings from birds and lower vertebrates to humans. The main differences between human and mouse/rat tail development relate to timing with, for example, formation of a new somite every 7 h in humans, compared with 2 h in mouse/rat, and termination of

tail elongation at the 36 to 37-somite stage in human, compared with the 65-somite stage in tailed rodents. While tail regression occurs completely in human embryos, it is noteworthy that the tail of mouse/rat embryos also regresses partially, with loss of secondary neural tube and tailgut, despite maintenance of an overall tail structure. An intriguing observation is the presence of secondary neural tube splitting in apparently normal human embryos, whereas this is seen only under pathological conditions in rodents. Future work in human embryos and organoids may shed light on the mechanisms(s) of this phenomenon.

MATERIALS AND METHODS

Human embryos

All embryos were obtained from the MRC/Wellcome Human Developmental Biology Resource (HDBR; www.hdbr.org) with UK ethics committee approval and written consent of donors. Embryos were collected on ice in L-15 medium, rinsed in phosphate buffered saline (PBS) and fixed overnight at 4ºC in 4% paraformaldehyde (PFA) in PBS. Embryos were assigned to Carnegie Stages (CS) using morphological criteria (O'Rahilly and Muller 1987; Bullen and Wilson 1997) and to 2-day post-conception intervals for regression analysis based on timings in Table 0-1 of O'Rahilly and Muller (1987). Only embryos that had normal external morphology and a normal karyotype were included in the study. Screening for aneuploidy was performed on all embryos, either by conventional karyotyping or by quantitative fluorescent polymerase chain reaction (QF-PCR) (Badenas et al., 2010).

Mouse embryos

Mouse studies were conducted under auspices of the UK Animals (Scientific Procedures) Act 1986 and the National Centre for the 3Rs' *Responsibility in the Use of Animals for Medical Research* (2019). Random-bred CD1 embryos were collected from pregnant females between embryonic days (E) 10.5 and 14.5 (E0.5 is the day of finding a copulation plug). Embryos were dissected in Dulbecco's modified Eagle's Medium (DMEM), rinsed in PBS, and fixed in 4% PFA overnight.

Embryo measurements

Measurements on human embryos were made post-fixation using an eyepiece graticule on a Zeiss SV6 stereo microscope. Crown-rump length was measured as the maximum distance from the top of the head to the base of the spine. Tail length was measured along the ventral surface, from the tail tip to the point where the tail joined the trunk. The distance from the tail tip to the caudal edge of the caudal-most somite was also measured. Somites were counted in total or, where indistinct more rostrally, the total number was estimated by considering the somite immediately rostral to the

hindlimb bud as somite 24. Analysis of PNP closure by somite stage (Figure 1I,J) was performed using archival embryo images, with PNP length measurements normalised to caudal somite length in the same embryo (both measured in pixels on photomicrographs).

H&E histology

PFA-fixed caudal embryonic regions were dissected away from the remainder of the embryo and dehydrated through an ascending alcohol series to Histoclear (National Diagnostics), embedded in 56ºC paraffin wax, and sectioned transversely at 7 µm thickness on a rotary microtome. For haematoxylin and eosin (H&E) staining, slides were dewaxed in Histoclear, and rehydrated through a descending alcohol series from 100% ethanol to water, then placed sequentially in: filtered Harris's haematoxylin (3 min); running tap water (1 min); Scott's Tap Water substitute (20 g sodium hydrogen carbonate + 3.5 g magnesium sulphate in 1L distilled water; ~3 sec); running tap water (1 min); 95% ethanol (1 min);eosin (3 min); running tap water (1 min); 95% ethanol (1 min); 100% ethanol (2 x 1 min); Histoclear (2x 5 min). Slides were mounted with DPX.

Immunohistochemistry

Initial studies used wax sections (Figure 3), and subsequently cryosections were used (Figure 4). For the latter, PFA-fixed tissue was dehydrated to 30% sucrose in PBS and stored at 4°C. Tissues were incubated for ~ 6 h in 30% sucrose + 7.5% gelatine in PBS at 56°C, positioned in the gelatine mix at room temperature and allowed to set, and stored at -80°C. Gelatine-embedded samples were sectioned on a cryostat at 15 µm thickness with a sample temperature of -23°C and an ambient temperature of -25°C. For staining, wax sections were rehydrated as for H&E, then blocked and incubated with antibodies as below. Cryosections were incubated in PBS at 37°C to melt the gelatine, and antigen retrieval was performed using a decloaking chamber. Slides were incubated at 110°C for 2 minutes in 10 mM sodium citrate + 0.05% Tween 20 in water (pH 6), and then returned to room temperature. Slides were rinsed in PBS + 0.1% Triton (PBST) and blocked for 1 h in PBST + 0.15% glycine + 10% sheep serum. Blocking solution was removed, followed by incubation overnight at 4°C in primary antibody solution: anti-cleaved caspase-3 (Asp175; Cell

Signalling, Cat. No. 9661) diluted in PBST + 1% sheep serum at 1:1000 for wax sections or 1:250 for cryosections. The next day, slides were washed 3 x for 5 min each in PBST, then incubated in a humidity chamber for 1 h in secondary antibody solution: 1:250 Alexa Fluor donkey anti-rabbit 568 (Thermo Fisher Scientific, Cat. No. A-11011). Slides were washed 3 x for 5 min in PBST, counterstained for 5 min in 1:5000 DAPI, washed a final 2 x 5 min in PBS, and mounted using ProLong Gold mountant (Thermo Fisher Scientific, Cat. No. P36930).

TUNEL staining

TdT-mediated dUTP-biotin nick end labelling (TUNEL; Apoptag) was performed according to manufacturer's instructions. Sections were counterstained with methyl green (Vector Labs, H-3402).

Morphometric analysis of embryo sections

All image analysis was carried out using Fiji Is Just ImageJ (FIJI) software (Schindelin et al., 2012). Area was calculated using the polygon tool. Nuclei were counted using the multi-point tool. Neural tube, notochord and tailgut areas, and tailgut nuclear number, were plotted against total area of the tail section, as a measure of position along the rostro-caudal axis.

Whole mount in situ hybridisation

Digoxygenin (DIG)-labelled mRNA probes for human *FGF8* (reference sequence NM_033165.5) and *WNT3A* (reference sequence NM_033131.4) were designed for *in situ* hybridisation. Human embryos or isolated caudal regions were fixed in 10% formalin, washed in PBS with 0.1% Tween (PBT), and processed for whole mount *in situ* hybridisation. Samples were bleached in 6% hydrogen peroxide, digested in a 5 μg/ml proteinase K - PBT solution, followed by a wash in 2 mg/ml glycine, and subsequently fixed in 0.2% glutaraldehyde made up in 4% paraformaldehyde. Samples were then incubated in pre-hybridisation mix (50% formamide, 1% sodium dodecyl sulfate (SDS), 5 x saline sodium citrate (SSC), 50 μg/ml yeast tRNA and 50 μg/ml heparin), and hybridised

with the corresponding digoxigenin (DIG)-labelled mRNA probes overnight at 70 °C. Hybridised probes were fixed using fixative wash solutions (solution 1: 50% formamide, 5x SSC and 1% SDS at 70 °C; and solution 2: 50% formamide, 2x SSC and 1% SDS at 65 °C). The samples were then blocked in 10% heat inactivated sheep serum, and incubated with anti-DIG-alkaline phosphatase antibody (Roche) solution. Developmental of the colour signal was carried out in nitrotetrazolium blue (NBT) and 5-bromo-4-chloro-3-indole (BCIP) solution. Whole mount images were taken using a DFC490 camera (Leica) connected to a Stemi SV11 stereomicroscope (Zeiss), and then embedded in gelatin-albumin for vibratome sectioning at a thickness of 40 μm. Sections were imaged using AxioVision v4.8.2 software on an Axioplan 2 microscope (Zeiss).

Systematic literature review (Supplementary Table 1)

PubMed (https://pubmed.ncbi.nlm.nih.gov/) was searched for a variety of term combinations that included: human; embryo; embryonic development; neuropore; primary neurulation; secondary neurulation; neural tube; organogenesis; tail; transcrptomics; gene expression. Retrieved papers were scanned for relevance sequentially using the title, abstract and full text, with non-qualifying papers dismissed at each stage. Additional relevant papers were identified from the bibliographies of the retrieved papers. Qualifying papers (n = 28) were those that presented original data on human low spinal/tail development, using embryo samples not described in other studies.

Statistical analysis

Linear regression analysis (Figure 1) and One-way ANOVA on ranks (Figure 2) were performed using Sigmaplot v14.5.

Acknowledgements

This work was supported in part by the Wellcome Human Developmental Biology Initiative (HDBI: grant 215116/Z/18/Z). Human embryonic material was provided by the MRC/Wellcome Human Developmental Biology Resource (grant MR/R006237/1; www.hdbr.org).

Table 1. Number of human embryos in the study, with breakdown by analysis type, sex and method of pregnancy termination *

Analysis type	Figures in paper	Total no.	No. females	No. males	No. sex unknown	No. medical	No. surgical
PNP morphology	1A-H	2 **	0	2	0	2	0
PNP closure timing	1I,J	40	24	16	0	40	0
Tail morphology, histology, cell death	2,3	37 **	14	21	2	36	1
Serial section analysis, cell death	4,6	11	5	6	0	10	1
FGF8, WNT3A expression	5	18	9	9	0	18	0
Totals		108	52	54	2	106	2

* Medical: mifepristone- and misoprostol-induced delivery; Surgical: ultrasound-guided vacuum aspiration.

** Embryos that are included in Table 2,

Table 2. Measurements of human embryos, CS12-18 *

Carnegie Stage (CS)	Age range (days post-fertilization)	Number of embryos	Somite number **	Crown-rump length ***	Tail length (total) ***	Tail length distal to somites ***
12	25-27	2	22, 22	3.0, 3.0	N/A	N/A
13	28-30	7	35.4 ± 2.3	6.4 ± 1.3	1.06 ± 0.44	0.49 ± 0.16
14	31-32	5	35.0 ± 2.0	8.4 ± 2.2	0.99 ± 0.21	0.56 ± 0.06
15	33-35	7	35.9 ± 1.8	8.9 ± 0.8	1.18 ± 0.55	0.67 ± 0.15
16	37-39	8	36.6 ± 2.6	11. 7 ± 1.2	1.29 ± 0.48	0.46 ± 0.13
17	40-43	4	32.3 ± 2.1	12.2 ± 1.2	1.18 ± 0.20	0.34 ± 0.01
18	44-45	6	32.6 ± 1.1	15.4 ± 2.2	1.14 ± 0.48	N/D

* Summary of embryos that underpin Figure 1A-H (CS12) and Figures 2 and 3 (CS13-18). For full data set, see Supplementary Table 1.

** Somite numbers: mean ± SD (except CS12, where actual somite numbers are shown). Somite number was available for all embryos except n = 5 at CS18.

*** Lengths (mm): mean ± SD (except CS12, where actual lengths are shown). Length measuements were available only for a sub-set of embryos. See Supplementary Table 1 for full details.

N/A: not applicable; N/D: not determined

REFERENCES

Agarwalla PK, Dunn IF, Scott RM, Smith ER. (2007) **Tethered cord syndrome** *Neurosurg Clin N Am*. **18**:531-547.

Amadei G, Handford CE, Qiu C, De Jonghe J, Greenfeld H, Tran M, Martin BK, Chen DY, Aguilera-Castrejon A, Hanna JH, Elowitz MB, Hollfelder F, Shendure J, Glover DM, Zernicka-Goetz M. (2022) **Embryo model completes gastrulation to neurulation and organogenesis** *Nature*. **610**:143-153.

Badenas C, Rodriguez-Revenga L, Morales C, Mediano C, Plaja A, Perez-Iribarne MM, Soler A, Clusellas N, Borrell A, Sanchez MA, Miro E, Sanchez A, Mila M, Jimenez W. (2010) **Assessment of qf-pcr as the first approach in prenatal diagnosis** *J Mol Diagn*. **12**:828-834.

Bolli R. (1966) **Sekundäre lumenbildungen im neuralrohr und rückenmark menschlicher embryonen** *Acta Anat*. **64**:48-81.

Brown NA, Fabro S. (1981) **Quantitation of rat embryonic development in vitro: A morphological scoring system** *Teratology*. **24**:65-78.

Bullen P, Wilson DI. (1997) **The carnegie staging of human embryos: A practical guide** In: Strachan T, Lindsay S, Wilson DI, editors. Molecular genetics of early human development. Oxford: BIOS Scientific Publishers Ltd. p. 27-50.

Butcher EO. (1929) **The development of the somites in the white rat (mus norvegicus albinus) and the fate of the myotomes, neural tube and gut in the tail** *Am J Anat*. **44**:381-439.

Cambray N, Wilson V. (2002) **Axial progenitors with extensive potency are localised to the mouse chordoneural hinge** *Development*. **129**:4855-4866.

Cambray N, Wilson V. (2007) **Two distinct sources for a population of maturing axial progenitors** *Development*. **134**:2829-2840.

Catala M. (2021) **Overview of secondary neurulation** *J Korean Neurosurg Soc*. **64**:346-358.

Cogliatti SB. (1986) **Diplomyelia: Caudal duplication of the neural tube in mice** *Teratology*. **34**:343-352.

Copp AJ, Adzick NS, Chitty LS, Fletcher JM, Holmbeck GN, Shaw GM. (2015) **Spina bifida** *Nat Rev Dis Primers*. **1**:15007.

Copp AJ, Seller MJ, Polani PE. (1982) **Neural tube development in mutant (curly tail) and normal mouse embryos: The timing of posterior neuropore closure in vivo and in vitro** *J Embryol Exp Morphol*. **69**:151-167.

Criley BB. (1969) **Analysis of the embryonic sources and mechanisms of development of posterior levels of chick neural tubes** *J Morph*. **128**:465-501.

Dady A, Havis E, Escriou V, Catala M, Duband JL. (2014) **Junctional neurulation: A unique developmental program shaping a discrete region of the spinal cord highly susceptible to neural tube defects** *J Neurosci*. **34**:13208-13221.

Denham M, Hasegawa K, Menheniott T, Rollo B, Zhang D, Hough S, Alshawaf A, Febbraro F, Ighaniyan S, Leung J, Elliott DA, Newgreen DF, Pera MF, Dottori M. (2015) **Multipotent caudal neural progenitors derived from human pluripotent stem cells that give rise to lineages of the central and peripheral nervous system** *Stem Cells*. **33**:1759-1770.

Diaz-Cuadros M, Wagner DE, Budjan C, Hubaud A, Tarazona OA, Donelly S, Michaut A, Al Tanoury Z, Yoshioka-Kobayashi K, Niino Y, Kageyama R, Miyawaki A, Touboul J, Pourquie O. (2020) **In vitro characterization of the human segmentation clock** *Nature*. **580**:113-118.

Dryden RJ. (1980) **Duplication of the spinal cord: A discussion of the embryogenesis of diplomyelia** *Dev Med Child Neurol*. **22**:234-243.

Eibach S, Moes G, Hou YJ, Zovickian J, Pang D. (2016) **Unjoined primary and secondary neural tubes: Junctional neural tube defect, a new form of spinal dysraphism caused by disturbance of junctional neurulation** *Childs Nerv Syst*. **33**:1633-1647.

Fallon JF, Simandl BK. (1978) **Evidence of a role for cell death in the disappearance of the embryonic human tail** *Am J Anat*. **152**:111-129.

Fang H, Yang Y, Li C, Fu S, Yang Z, Jin G, Wang K, Zhang J, Jin Y. (2010) **Transcriptome analysis of early organogenesis in human embryos** *Dev Cell*. **19**:174-184.

Fedorova V, Vanova T, Elrefae L, Pospisil J, Petrasova M, Kolajova V, Hudacova Z, Baniariova J, Barak M, Peskova L, Barta T, Kaucka M, Killinger M, Vecera J, Bernatik O, Cajanek L, Hribkova H, Bohaciakova D. (2019) **Differentiation of neural rosettes from human pluripotent stem cells in vitro is sequentially regulated on a molecular level and accomplished by the mechanism reminiscent of secondary neurulation** *Stem Cell Res*. **40**:101563.

Gajovic S, Kostovic-Knezevic L, Svajger A. (1989) **Origin of the notochord in the rat embryo tail** *Anat Embryol*. **179**:305-310.

Gajovic S, Kostovic-Knezevic L, Svajger A. (1993) **Morphological evidence for secondary formation of the tail gut in the rat embryo** *Anat Embryol (Berl)*. **187**:291-297.

Garriock RJ, Chalamalasetty RB, Zhu J, Kennedy MW, Kumar A, Mackem S, Yamaguchi TP. (2020) **A dorsal-ventral gradient of wnt3a/beta-catenin signals controls mouse hindgut extension and colon formation** *Development*. **147**.

Gonzalez-Gobartt E, Blanco-Ameijeiras J, Usieto S, Allio G, Benazeraf B, Marti E. (2021) **Cell intercalation driven by smad3 underlies secondary neural tube formation** *Dev Cell*. **56**:1147-1163 e1146.

Henrique D, Abranches E, Verrier L, Storey KG. (2015) **Neuromesodermal progenitors and the making of the spinal cord** *Development*. **142**:2864-2875.

Hughes AF, Freeman RB. (1974) **Comparative remarks on the development of the tail cord among higher vertebrates** *J Embryol Exp Morphol*. **32**:355-363.

Jolly J, Ferester-Tadie M. (1936) **Recherches sur l'oeuf du rat et de la souris** *Arch d'Anat Microsc*. **32**:323-390.

Jones VJ, Greene NDE, Copp AJ. (2019) **Genetics and developmental biology of closed dysraphic conditions** In: Tubbs RS, Oskouian RJ, Blount JP, Oakes WJ, editors. Occult spinal dysraphism. Springer. p. 325-344.

Karzbrun E, Khankhel AH, Megale HC, Glasauer SMK, Wyle Y, Britton G, Warmflash A, Kosik KS, Siggia ED, Shraiman BI, Streichan SJ. (2021) **Human neural tube morphogenesis in vitro by geometric constraints** *Nature*. **599**:268-272.

Kostovic-Knezevic L, Gajovic S, Svajger A. (1991) **Morphogenetic features in the tail region of the rat embryo** *Int J Dev Biol*. **35**:191-195.

Krupp DR, Xu PT, Thomas S, Dellinger A, Etchevers HC, Vekemans M, Gilbert JR, Speer MC, Ashley-Koch AE, Gregory SG. (2012) **Transcriptome profiling of genes involved in neural tube closure during human embryonic development using long serial analysis of gene expression (long-sage)** *Birth Defects Res A Clin Mol Teratol*. **94**:683-692.

Kunitomo K. (1918) **The development and reduction of the tail and of the caudal end of the spinal cord** *Carnegie Inst Contr Embryol*. **8**:161-198.

Lemire RJ. (1969) **Variations in development of the caudal neural tube in human embryos (horizons xiv-xxi)** *Teratology*. **2**:361-370.

Libby ARG, Joy DA, Elder NH, Bulger EA, Krakora MZ, Gaylord EA, Mendoza-Camacho F, Butts JC, McDevitt TC. (2021) **Axial elongation of caudalized human organoids mimics aspects of neural tube development** *Development*. **148**:dev 198275.

Matsuda M, Yamanaka Y, Uemura M, Osawa M, Saito MK, Nagahashi A, Nishio M, Guo L, Ikegawa S, Sakurai S, Kihara S, Maurissen TL, Nakamura M, Matsumoto T, Yoshitomi H, Ikeya M, Kawakami N, Yamamoto T, Woltjen K, Ebisuya M, Toguchida J, Alev C. (2020) **Recapitulating the human segmentation clock with pluripotent stem cells** *Nature*. **580**:124-129.

McShane SG, Mole MA, Savery D, Greene ND, Tam PP, Copp AJ. (2015) **Cellular basis of neuroepithelial bending during mouse spinal neural tube closure** *Dev Biol*. **404**:113-124.

Miller SA, Briglin A. (1996) **Apoptosis removes chick embryo tail gut and remnant of the primitive streak** *Dev Dyn*. **206**:212-218.

Moris N, Anlas K, van den Brink SC, Alemany A, Schroder J, Ghimire S, Balayo T, van Oudenaarden A, Martinez Arias A. (2020) **An in vitro model of early anteroposterior organization during human development** *Nature*. **582**:410-415.

Müller F, O'Rahilly R. (1987) **The development of the human brain, the closure of the caudal neuropore, and the beginning of secondary neurulation at stage 12** *Anat Embryol*. **176**:413-430.

Müller F, O'Rahilly R. (2004) **The primitive streak, the caudal eminence and related structures in staged human embryos** *Cells Tissues Organs*. **177**:2-20.

Nievelstein RA, Hartwig NG, Vermeij-Keers C, Valk J. (1993a) **Embryonic development of the mammalian caudal neural tube** *Teratology*. **48**:21-31.

Nievelstein RAJ, Hartwig NG, Vermeij-Keers C, Valk J. (1993b) **Embryonic development of the mammalian caudal neural tube** *Teratology*. **48**:21-31.

Nikolopoulou E, Galea GL, Rolo A, Greene ND, Copp AJ. (2017) **Neural tube closure: Cellular, molecular and biomechanical mechanisms** *Development*. **144**:552-566.

O'Rahilly R, Muller F. (1987) **Developmental stages in human embryos**. Washington: Carnegie Institute of Washington, Publication 637.

O'Rahilly R, Müller F. (2002) **The two sites of fusion of the neural folds and the two neuropores in the human embryo** *Teratology*. **65**:162-170.

Olivera-Martinez I, Harada H, Halley PA, Storey KG. (2012) **Loss of fgf-dependent mesoderm identity and rise of endogenous retinoid signalling determine cessation of body axis elongation** *PLoS Biol*. **10**:e1001415.

Pang D. (2020) **Perspectives on spinal dysraphism : Past, present, and future** *J Korean Neurosurg Soc*. **63**:366-372.

Pytel A, Bruska M, Wozniak W. (2007) **Evidence that the caudal portion of the neural tube develops by cavitation of a neural cord in the caudal eminence of human embryos** *Folia Morphol (Warsz)*. **66**:104-108.

Qi BQ, Beasley SW, Williams AK, Fizelle F. (2000) **Apoptosis during regression of the tailgut and septation of the cloaca** *J Pediatr Surg*. **35**:1556-1561.

Rifes P, Isaksson M, Rathore GS, Aldrin-Kirk P, Moller OK, Barzaghi G, Lee J, Egerod KL, Rausch DM, Parmar M, Pers TH, Laurell T, Kirkeby A. (2020) **Modeling neural tube development by differentiation of human embryonic stem cells in a microfluidic wnt gradient** *Nat Biotechnol*. **38**:1265-1273.

Saitsu H, Yamada S, Uwabe C, Ishibashi M, Shiota K. (2004) **Development of the posterior neural tube in human embryos** *Anat Embryol (Berl)*. **209**:107-117.

Sapunar D, Vilovic K, England M, Saraga-Babic M. (2001) **Morphological diversity of dying cells during regression of the human tail** *Ann Anat*. **183**:217-222.

Schindelin J, Arganda-Carreras I, Frise E, Kaynig V, Longair M, Pietzsch T, Preibisch S, Rueden C, Saalfeld S, Schmid B, Tinevez JY, White DJ, Hartenstein V, Eliceiri K, Tomancak P, Cardona A. (2012) **Fiji: An open-source platform for biological-image analysis** *Nat Methods*. **9**:676-682.

Schoenwolf GC. (1984) **Histological and ultrastructural studies of secondary neurulation of mouse embryos** *Am J Anat*. **169**:361-374.

Schoenwolf GC, De Longo J. (1980) **Ultrastructure of secondary neurulation in the chick embryo** *Am J Anat*. **158**:43-63.

Shum ASW, Copp AJ. (1996) **Regional differences in morphogenesis of the neuroepithelium suggest multiple mechanisms of spinal neurulation in the mouse** *Anat Embryol*. **194**:65-73.

Stiefel D, Copp AJ, Meuli M. (2007) **Fetal spina bifida: Loss of neural function in utero** *J Neurosurg*. **106**:213-221.

Streeter GL. (1919) **Factors involved in the formation of the filum terminale** *Am J Anat*. **25**:1-11.

Svajger A, Kostovic-Knezevic L, Bradamante Z, Wrischer M. (1985) **Tail gut formation in the rat embryo** *Roux's Arch Dev Biol*. **194**:429-432.

Tam PP. (1981) **The control of somitogenesis in mouse embryos** *J Embryol Exp Morphol*. **65 Suppl**:103-128.

Tam PPL. (1984) **The histogenetic capacity of tissues in the caudal end of the embryonic axis of the mouse** *J Embryol Exp Morphol*. **82**:253-266.

Tzouanacou E, Wegener A, Wymeersch FJ, Wilson V, Nicolas JF. (2009) **Redefining the progression of lineage segregations during mammalian embryogenesis by clonal analysis** *Dev Cell*. **17**:365-376.

Van Straaten HWM, Hekking JWM, Copp AJ, Bernfield M. (1992) **Deceleration and acceleration in the rate of posterior neuropore closure during neurulation in the curly tail (ct) mouse embryo** *Anat Embryol*. **185**:169-174.

Vilovic K, Ilijic E, Glamoclija V, Kolic K, Bocina I, Sapunar D, Saraga-Babic M. (2006) **Cell death in developing human spinal cord** *Anatomy and Embryology*. **211**:1-9.

Wilson V, Olivera-Martinez I, Storey KG. (2009) **Stem cells, signals and vertebrate body axis extension** *Development*. **136**:1591-1604.

Wymeersch FJ, Wilson V, Tsakiridis A. (2021) **Understanding axial progenitor biology in vivo and in vitro** *Development*. **148**:dev.180612.

Xia B, Zhang W, Zhao G, Zhang X, Bai J, Brosh R, Wudzinska A, Huang E, Ashe H, Ellis G, Pour M, Zhao Y, Coelho C, Zhu Y, Miller A, Dasen JS, Maurano MT, Kim SY, Boeke JD, Yanai I. (2024) **On the genetic basis of tail-loss evolution in humans and apes** *Nature*. **626**:1042-1048.

Xu Y, Zhang T, Zhou Q, Hu M, Qi Y, Xue Y, Nie Y, Wang L, Bao Z, Shi W. (2023) **A single-cell transcriptome atlas profiles early organogenesis in human embryos** *Nat Cell Biol*. **25**:604-615.

Yang HJ, Lee DH, Lee YJ, Chi JG, Lee JY, Phi JH, Kim SK, Cho BK, Wang KC. (2014) **Secondary neurulation of human embryos: Morphological changes and the expression of neuronal antigens** *Childs Nerv Syst*. **30**:73-82.

Yang HJ, Wang KC, Chi JG, Lee MS, Lee YJ, Kim SK, Cho BK. (2003) **Neural differentiation of caudal cell mass (secondary neurulation) in chick embryos: Hamburger and hamilton stages 16-45** *Developmental Brain Research*. **142**:31-36.

Yi H, Xue L, Guo MX, Ma J, Zeng Y, Wang W, Cai JY, Hu HM, Shu HB, Shi YB, Li WX. (2010) **Gene expression atlas for human embryogenesis** *FASEB J*. **24**:3341-3350.

Santos et al – Revised figures

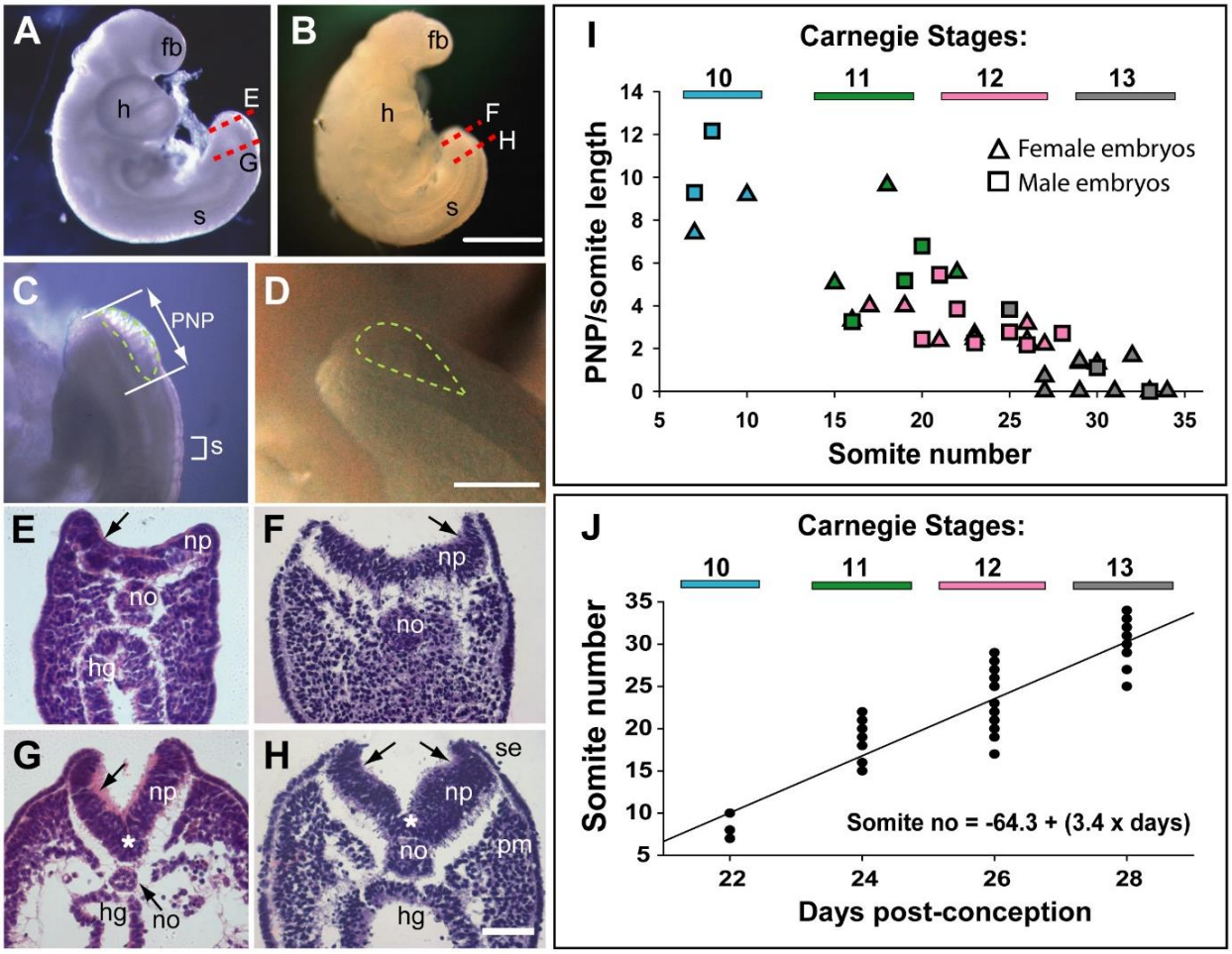

Figure 1. Morphology and timing of human posterior neuropore (PNP) closure. (**A,B**) Two CS12 embryos viewed from right side, each with 22-23 somites (s), and a looped heart (h). Neural tube closure is complete along most of the body axis, including the forebrain (fb), whereas the PNP remains open caudally. (**C,D**) Magnified oblique views from upper right side of the caudal region; the open PNP is outlined with dashed lines. (**E-H**) H&E-stained transverse sections, through the PNP, with section planes as indicated by dashed lines in A, B. The most caudally located sections (E,F) show a relatively flat neural plate (np), although incipient dorsolateral hinge points (DLHPs; arrows) are visible. Note the midline notochord (no) underlying the neural plate, and hindgut (hg) beneath the notochord (in E only). More rostral sections (G,H) show elevated neural folds with DLHPs clearly visible (arrows: unilateral in G, bilateral in H), located where basal contact of the neural plate changes from surface ectoderm (se), to paraxial mesoderm (pm). A median hinge point (MHP; asterisks in G,H) overlies the notochord. (**I**) PNP length (double headed arrow in C), normalised to somite (s) length (bracketed in C), determined from photographic images of 40 human embryos (24

females; 16 males) at CS10 (n = 4), CS11 (n = 8), CS12 (n = 16) and CS13 (n = 12). Symbol colours indicate the Carnegie Stages assigned at the time of collection. The PNP shows gradual closure, with completion around the 30 somite stage. (**J**) Somite number of the 40 embryos in I, plotted against days post-conception, as reported for each Carnegie Stage by O'Rahilly and Muller (1987). The linear regression equation is shown, with $R^2 = 0.82$, and $p < 0.001$. Scale bars: 1 mm in A,B; 0.4 mm in C,D; 0.1 mm in E-H.

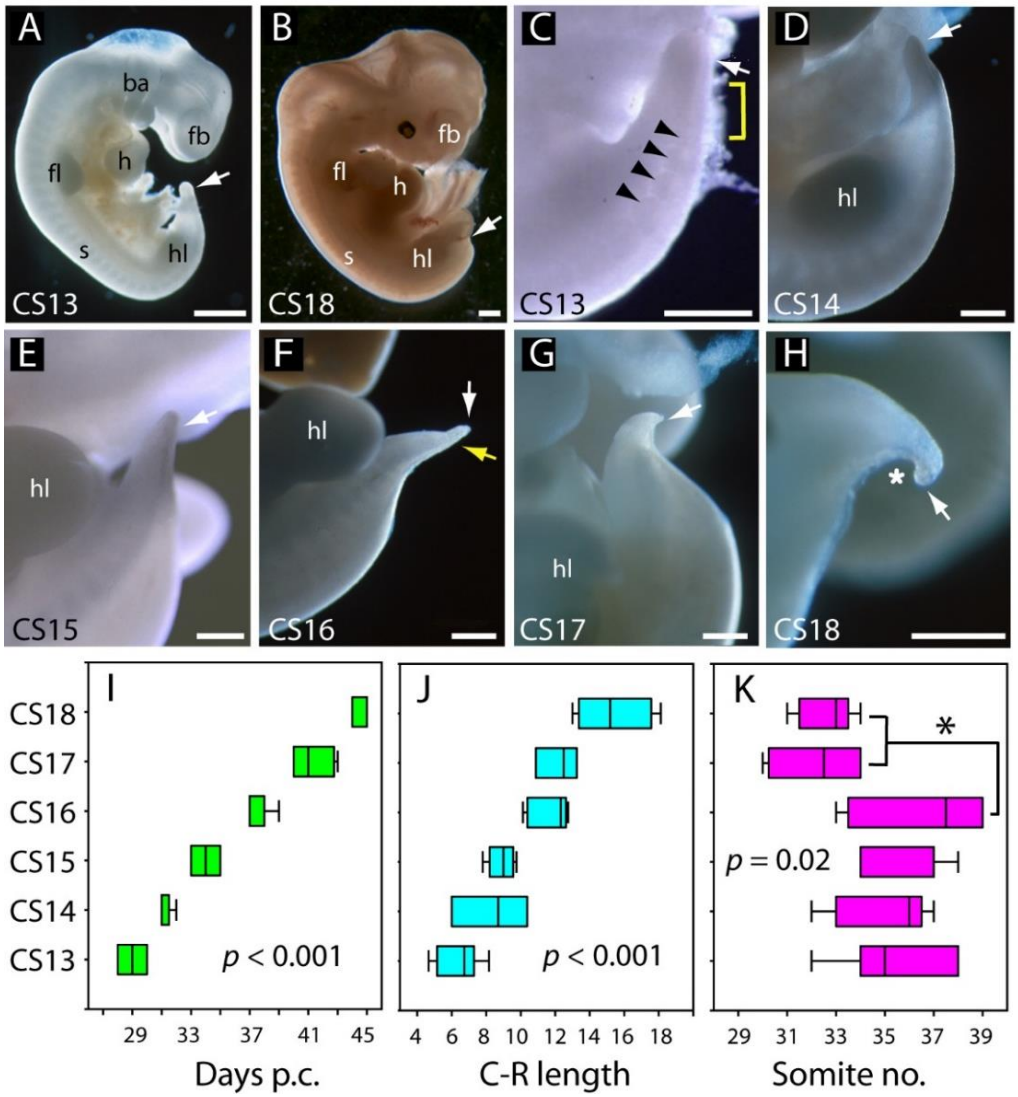

Figure 2. Development of the tail in human embryos. (**A,B**) Whole embryos at CS13 (A) and CS18 (B), showing the range of stages studied (4-6.5 weeks post-conception). The tail bud (arrow) is well formed at CS13 following completion of PNP closure at CS12, whereas, by CS18, tail development and regression are largely complete and only a small tail remnant remains (arrow). (**C-H**) Higher magnification views of the caudal region at CS13 to CS18. At CS13, the tail bud is relatively massive, tapering gradually and with a rounded end (arrow in C). Somites are visible rostral to the tail bud (arrowheads) with an intervening region of presomitic mesoderm (yellow bracket). At CS14 and CS15 the tail narrows progressively, with distal tapering (arrows in D-E). By CS16, this has yielded a slender structure with a narrow pointed end (white arrow in F) in which somites extend almost to the tail tip (yellow arrow in F). Thereafter, the tail shortens progressively (arrows in G,H), develops a marked flexion (asterisk in H), and becomes increasingly translucent (G,H). (**I-K**) Analysis of embryos in the range CS13-CS16 (Table 2), plotting CS against: (I) days post-conception

(p.c., see Materials & Methods), (J) crown-rump (C-R) length in mm, and (K) somite no. One-way ANOVA on ranks shows all three parameters vary significantly with CS (*p*-values on graphs). Somite no. reduces significantly between CS16 and CS17/18 (* $p < 0.05$). Abbreviations: ba, branchial arches; fb, forebrain; fl, forelimb; h, heart; hl, hindlimb; s, somites. Scale bars: 1 mm in A,B; 0.5 mm in C-H.

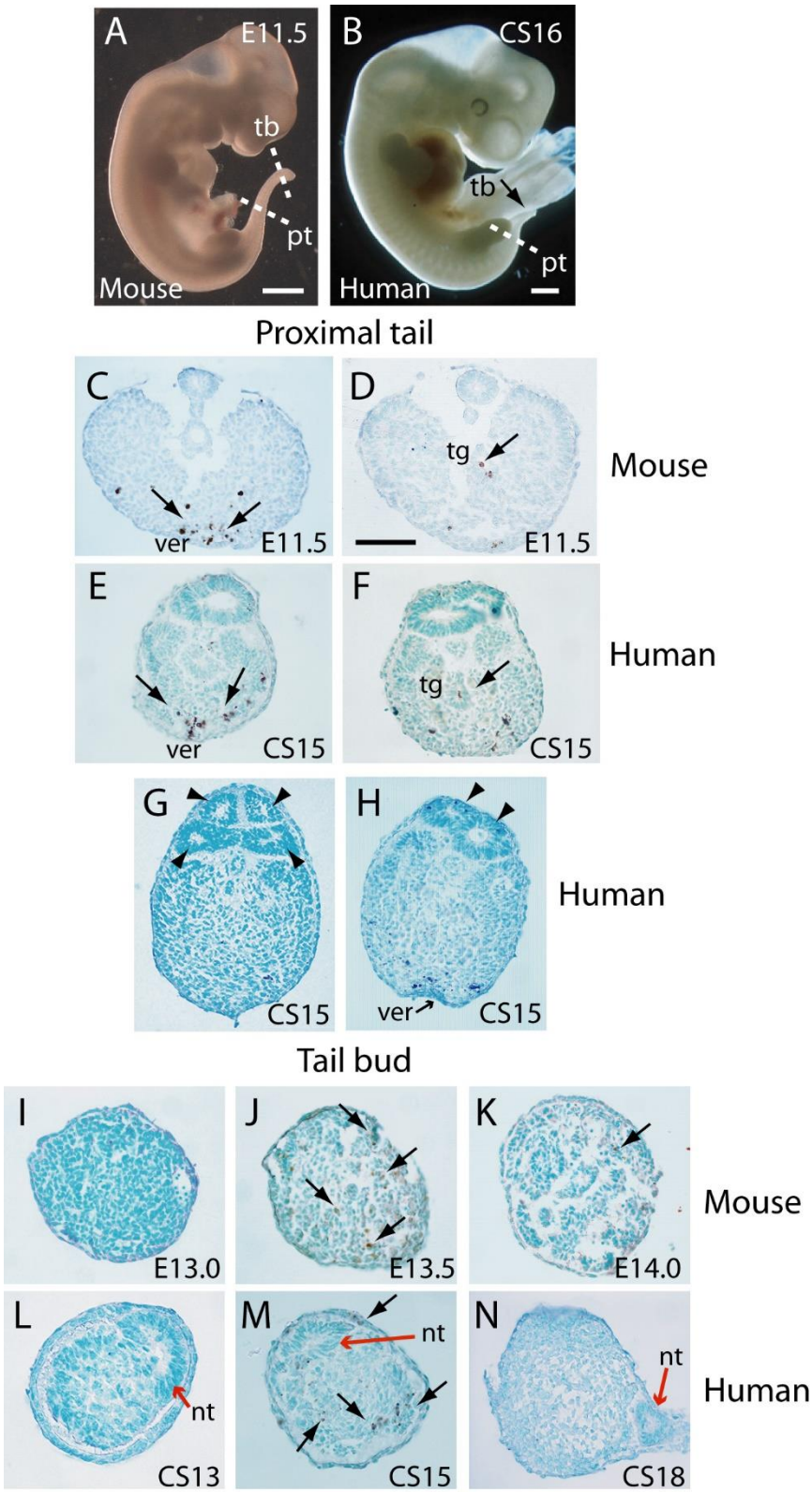

Figure 3. Tail morphology and apoptosis in mouse and human embryos. (**A,B**) Mouse E11.5 (A) and human CS16 (B) embryos to illustrate the level of transverse sections through the proximal tail (pt) and tailbud (tb) regions of mouse (C,D,I-K) and human (E-H,L-N) embryos

at the stages indicated on the panels. Immunohistochemistry was performed on paraffin wax sections for activated caspase 3 (brown stain), with counterstaining by methyl green. (**C-F**) In the proximal tail region, intense programmed cell death is observed in the ventral midline mesoderm overlying the ventral ectodermal ridge (ver) of both mouse (arrows in C) and human (arrows in E) embryos. Cell death can also be detected in the tailgut (tg) of both mouse (arrow in D) and human embryos (arrow in F). C,D are sections from a single E11.5 mouse embryo; E,F are sections from a single CS15 human embryo. (**G,H**) Multiple neural tube profiles in two human embryonic tails at CS15: four lumens are visible in one embryo (arrowheads in G) and two lumens in a second (arrowheads in H). (**I-K**) In mouse, the tail bud displays a stage-dependent burst of apoptotic cell death at E13.5 (arrows in J), with absence of caspase 3-positive cells 12 h earlier, at E13.0 (I), and only occasional dying cells 12 h later, at E14.0 (arrow in K). Note the absence of a neural tube at the mouse tail bud tip, and the sparse nature of the tail bud mesenchyme at E14.0. (**L-N**) Human embryonic tail buds show a similar developmental sequence to the mouse, with absence of cell death at CS13 (L), abundant dying cells at CS15 (arrows in M) and cessation of cell death by CS18 (N). Unlike the mouse, the secondary neural tube extends to the tail bud tip (red arrows in L-N), and this terminal neural tube portion has a single lumen in all three embryos. Scale bars in A,B, 1 mm; bar in C represents: 70 µm (C,D), 50 µm (E-K,N) and 30 µm (L,M).

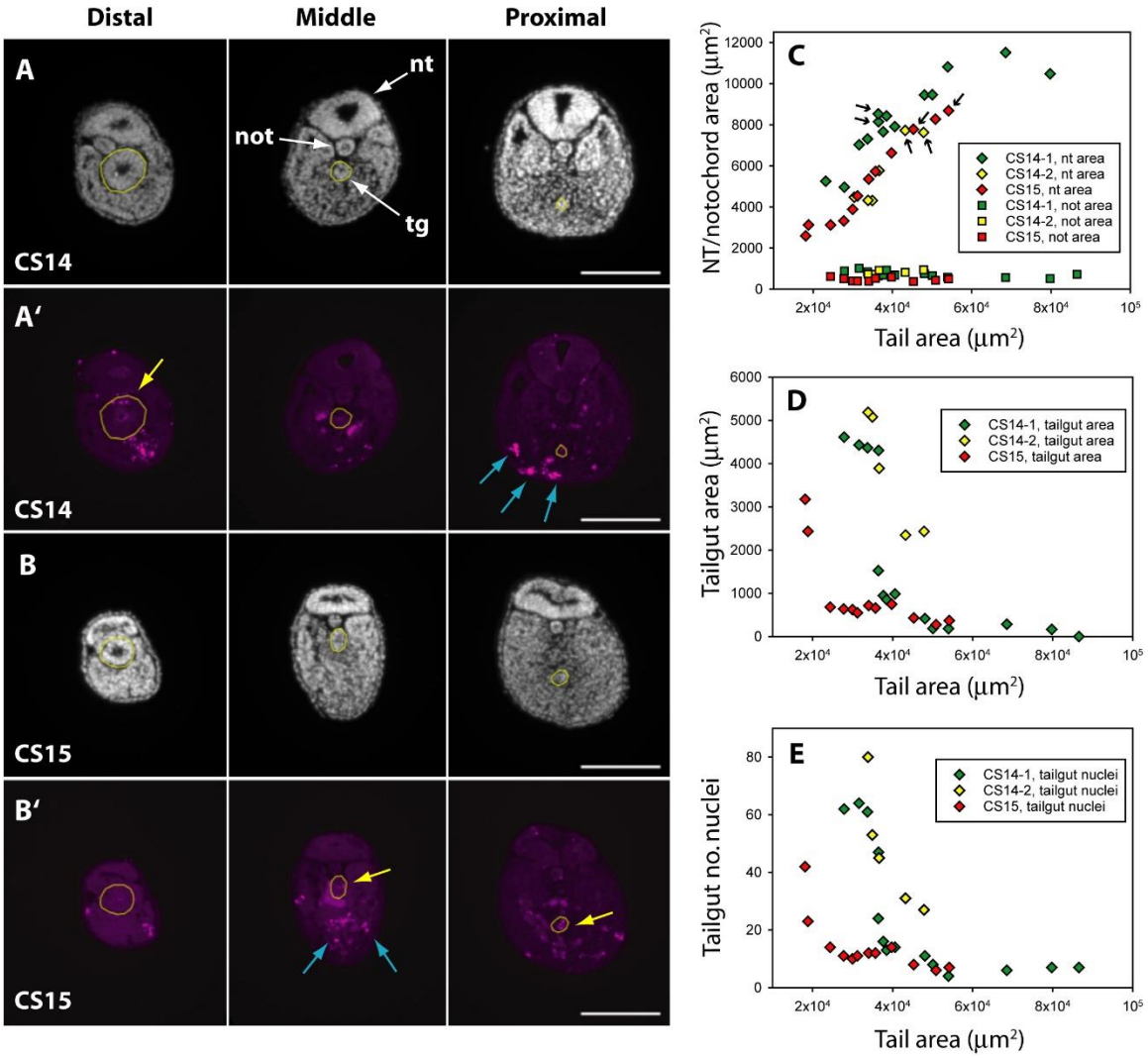

Figure 4. Programmed cell death and tissue size along the developing human tail. (**A,A',B,B'**) Transverse sections at distal (left), middle (centre) and proximal (right) levels of the tail. Panels show DAPI (A,B) and anti-cleaved caspase 3 immunostaining (A',B') of the same sections at CS14 (A,A') and CS15 (B,B'). Yellow dotted lines outline the tailgut. Apoptotic cell death occurs mainly in tailgut (tg, yellow arrows) and ventral mesoderm (blue arrows). Note the diminishing diameter of the tailgut from distal to proximal. (**C**) Change in transverse sectional areas of neural tube (nt, diamonds) and notochord (not, squares) along the body axis in CS14 (x 2; green and yellow symbols) and CS15 (red symbols) embryos. Embryos CS14-1 and CS15 are shown in (A,B). Tissue-specific areas (y-axis) are plotted against total tail area (x-axis), which increases from left (distal sections) to right (proximal sections). In all embryos, neural tube area increases in a proximal direction, whereas notochord area is relatively constant along the axis. Arrows: sections in which neural tube shows multiple lumens (see Figure 6). (**D,E**) Similar analysis for tailgut area (D) and tailgut nuclear number (E). Both show a dramatic reduction in a distal-to-proximal direction, in contrast to neural tube and notochord. Scale bars: 50 μm.

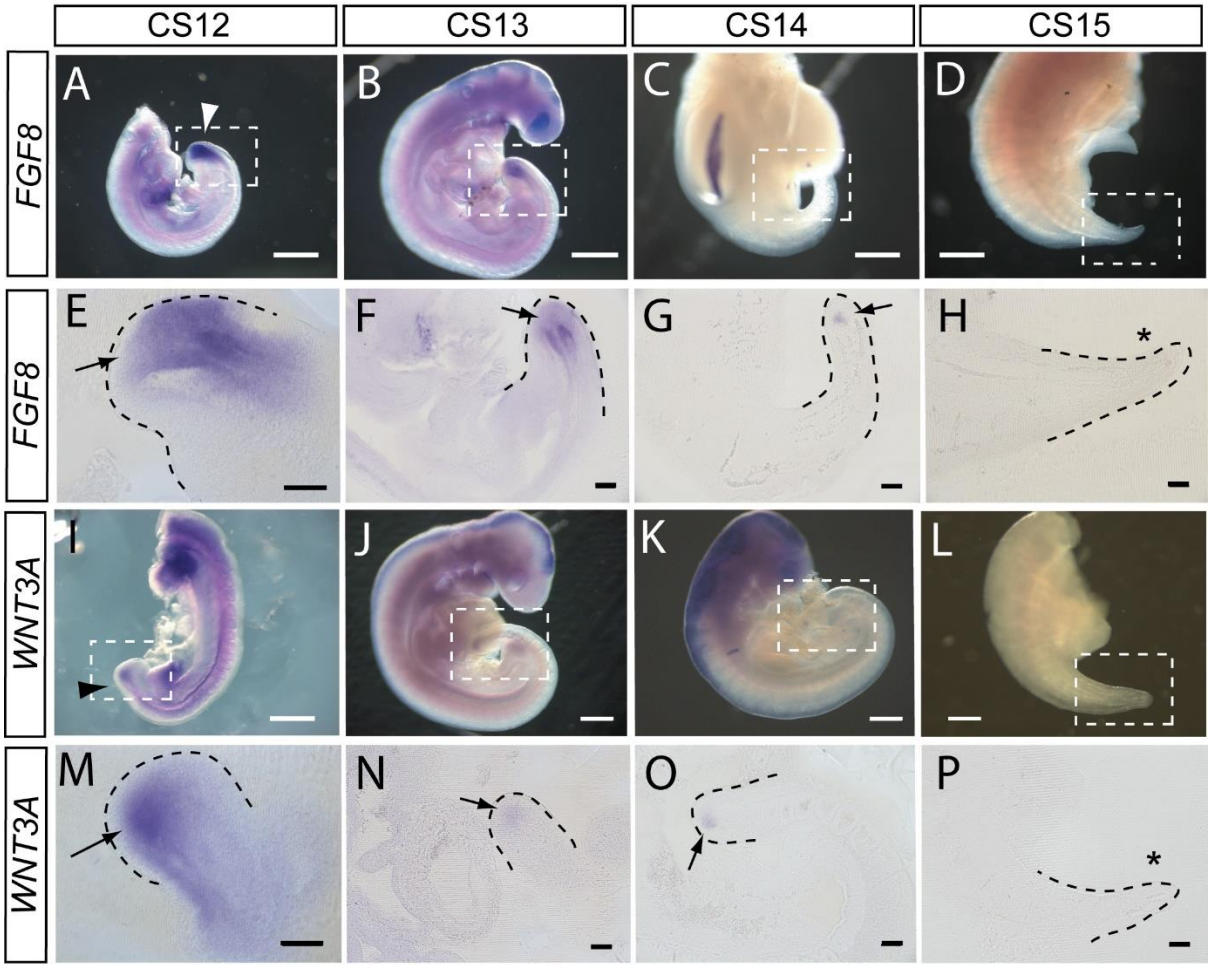

Figure 5. *FGF8* and *WNT3A* expression in the elongating caudal region of human embryos. Whole mount *in situ* hybridisation (A-D, I-L) and sagittal vibratome sections through the caudal region (E-H, M-P) for *FGF8* (A-H) and *WNT3A* (I-P) in embryos at CS12 (A,E,I,M), CS13 (B,F,J,N), CS14 (C,G,K,O) and CS15 (D,H,L,P). Both genes show prominent expression domains in the tail bud at CS12 (arrows in E,M) when axial elongation is underway and the posterior neuropore (PNP) is closing (arrowheads in A,I). At CS13, following PNP closure, expression of *FGF8* and *WNT3A* remains prominent although less intense and more localised to the terminal tail bud than at CS12 (arrows in F,N). By CS14, both genes exhibit much smaller, highly localised expression domains that each appears as a 'dot' within the tail bud region (arrows in G,O). By CS15, axial elongation has ceased, the tail tip has narrowed and is increasingly transparent. At this stage, expression of neither gene can be detected (asterisks in H,P). Whole embryos shown in B,J,K; isolated trunk/caudal regions shown in A,C,D,I,L. No. embryos analysed: FGF8, n = 2 for each stage; WNT3A, n = 2 for each stage except n = 3 for CS13. Scale bars: A-D, I-L, 1 mm; E-H, M-P, 100 µm.

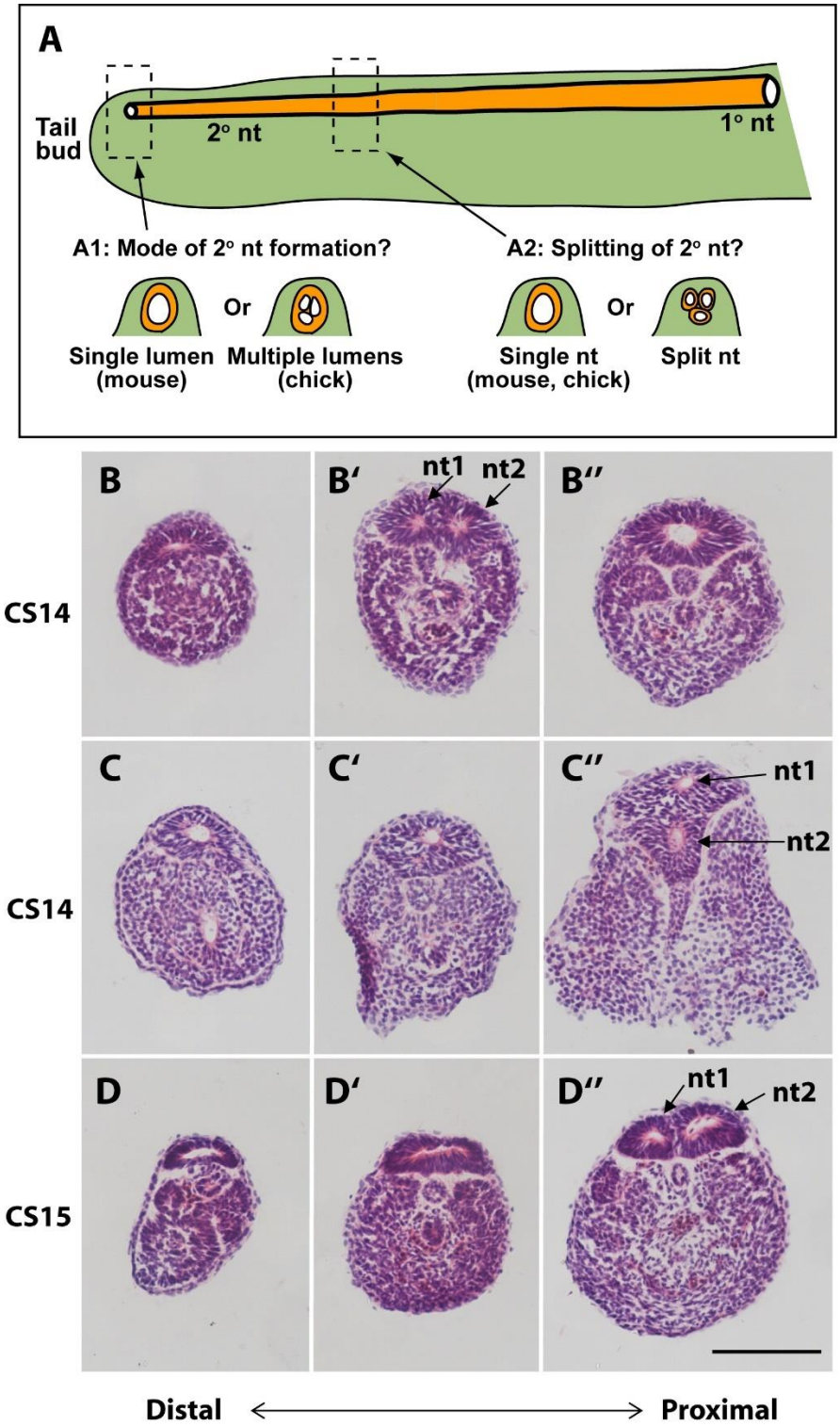

Figure 6. Mode of formation and proximal splitting of the human secondary neural tube. (**A**) Hypotheses on mode of formation of the human secondary neural tube (2° nt). A single lumen may be formed in the tail bud as in mouse or, by analogy to chick, multiple lumens may form initially, which then coalesce to form the secondary neural tube (A1). Alternatively, the finding of multiple neural tube lumens in sections of some human tails may reflect splitting of

the secondary neural tube at more rostral levels (A2). (**B-D’’**) Representative serial transverse sections (haematoxylin and eosin) through three human embryonic tails at CS14 (x 2; B,C) and CS15 (D). Sections close to the tail bud tip (left side: B,C,D) show a broad, dorsoventrally flattened neural tube with a single lumen. There is no evidence of multiple lumens coalescing in the tail bud of any embryos. Further rostrally (middle and right side panels: B’,B’’,C’,C’’,D’,D’’), some sections show a neural tube with single lumen (C’,D’), whereas others show evidence of secondary neural tube splitting, with two lumens (nt1, nt2 in B’,C’’,D’’). One CS14 embryo shows re-establishment of a single lumen in more proximal sections (B’’), after splitting more distally (B’). These findings support a mouse-like formation of the human secondary neural tube with, additionally, splitting at various rostro-caudal levels along the tail. Scale bar: 50 µm.